

DETERMINATION OF THE MECHANICAL CHARACTERISTICS AND SPECIFIC FRACTURE ENERGY OF THERMALLY HARDENED REINFORCEMENT

Q. Zhang,¹ Yu. V. Mol'kov,^{2,3} Yu. M. Sobko,⁴ Ya. Z. Blikhars'kyi,⁴ and R. E. Khmil'⁴

The results of experimental investigations and the method of digital image correlation are used to investigate the variations of the mechanical characteristics of the material of thermally hardened steel reinforcement across the thickness of a bar. The conventional and true stress–strain diagrams of the solid reinforcement and standard specimens made of this reinforcement are plotted. We determine the specific fracture energy for different zones of thermally hardened reinforcement. The necessity of taking into account the variations of the mechanical characteristics across the thickness of the bar in the design of building structures and the advantages of application of the specific fracture energy as an invariant characteristic of the material are demonstrated.

Keywords: reinforcement, steel, mechanical characteristics, digital image correlation, true fracture diagram, fracture energy.

In the design of reinforced concrete structural elements, their load-bearing capacity is determined with regard for the physicomaterial characteristics of the reinforcement bars. In this case, it is important to use well-substantiated procedures for the reliable evaluation of the load-bearing capacity of building structural elements and, in particular, of the beams, floor slabs, etc., especially in the case where they are strengthened by thermally hardened reinforcement. For this type of reinforcement, the variations the mechanical characteristics across the thickness of the bar are typical.

To determine the mechanical characteristics of reinforcement bars, we use cylindrical specimens tested by the standard methods [1–3]. To produce these specimens, the outer hardened layer of the metal is removed from the reinforcement and, hence, the mechanical characteristics of the core of the reinforcement bar are attained. The solid reinforcement bars are also tested and their characteristics are determined from the fracture diagrams plotted on the “conventional-stress σ –relative elongation δ ” coordinates without determination of the true stresses and strains.

In what follows, on the basis of the results of testing of the specimens of different diameters prepared by turning thermally hardened reinforcement bars, we determine the mechanical characteristics of different zones of the material of reinforcement. To plot the stress–strain diagrams on the conventional and true coordinates, we used the contemporary high-precision method of measuring displacements and strains, namely, the digital image correlation (DIC) method [4, 5].

The aim of the present work is to study the deformation and fracture of thermally hardened reinforcements and determine the variations of its mechanical characteristics across the thickness of the bar with an aim to make a well-justified choice of these characteristics in the numerical analysis of elements of the reinforced-concrete structures.

¹ Yangtze University, China.

² Corresponding author; e-mail: dep-12@ipm.lviv.ua.

³ Karpenko Physicomaterial Institute, Ukrainian National Academy of Sciences, Lviv, Ukraine.

⁴ “L'viv's'ka Politekhnikha” National University, Lviv, Ukraine.

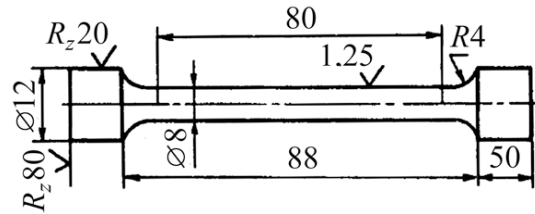


Fig. 1. Standard cylindrical specimen for the determination of mechanical characteristics.

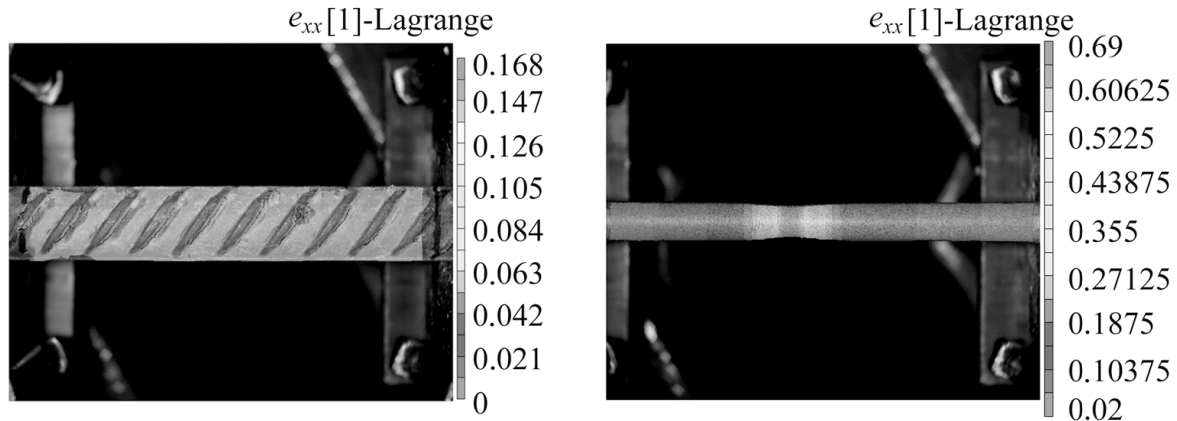


Fig. 2. Strain distributions on the surfaces of a reinforcement bar (a) and a cylindrical specimen (b) under the critical load obtained by the method of digital image correlation.

Method of Investigation

We used three types of specimens: type I is an untreated reinforcement bar with a diameter of 12 mm, whose total length is 200 mm, and the length of its working part is equal to 120 mm; type II and type III are standard cylindrical specimens (Fig. 1) with diameters of 10 and 8 mm and the length of the working zone equal to 100 and 80 mm, respectively. All specimens were made from the same reinforcement bar.

The specimens were stretched in a tensile testing machine up to fracture for a speed of motion of the moving crossarm equal to 2 mm/min. We recorded the loading force by a built-in strain gauge of the FPZ-100 machine, whereas the elongation was recorded with the help of a strain-gauge extensometer. The signals from the strains gauge and the extensometer were recorded with the use of an analog-to-digital converter (ADC) and stored in a personal computer.

At the same time, we used a Toupcam UCMOS 10000KPA commercial digital camera rigidly fixed on the immobile crossarm of the FPZ-100 machine to make the images of the specimen surface in the process of its deformation. The images were used for processing by the DIC method. Their resolution was 10 MP (3584 × 2748 pixels) in the *bmp format. Under loading, we made series of photographs of an area of the specimen surface; the first frame corresponded to the onset of loading, and the frequency of taking photos (1 fps) was equal to the frequency of recording of the loading force by the ADC. The indicated frequency of taking photos makes it possible to determine the force applied to the specimen at the time of recording of each frame with a sufficiently high accuracy and is sufficient for making images at the times close to the fracture of the specimen. In testing the specimens, we obtained an array of images (150–200 pieces for each specimen). As a result of processing of these images by the DIC method, we established the distributions of displacements and strains in each stage of loading (Fig. 2).

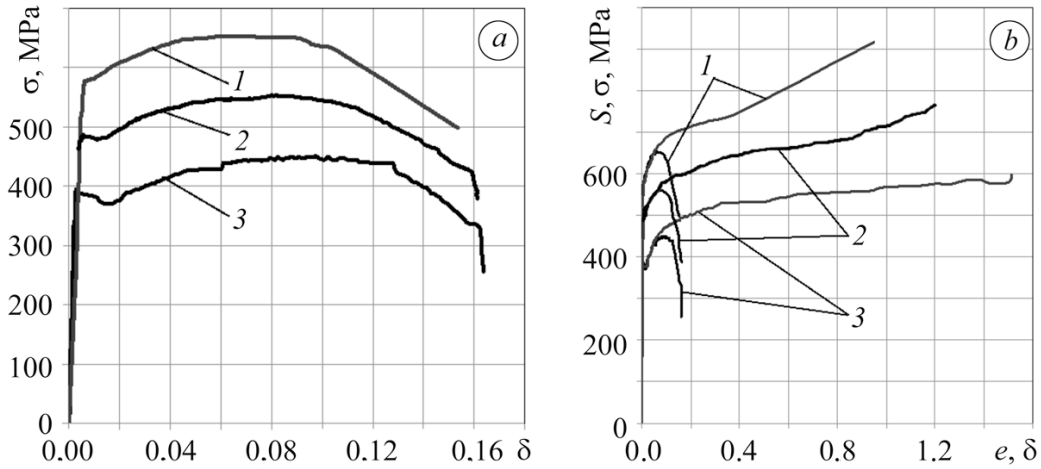


Fig. 3. Conventional (a) and true (b) stress-strain diagrams of the material of reinforcement: (1) untreated reinforcement bar (type I); (2) specimen 10 mm in diameter (type II); (3) specimen 8 mm in diameter (type III).

Results and Discussion

The loading force P and the elongation of the working part of a specimen Δl were used to find the conventional stresses $\sigma = P/F_0$ (where F_0 is the initial cross-sectional area of the reinforcement bar or of a cylindrical specimen) and relative elongation $\delta = \Delta l/l_0$ (where l_0 is the initial working length of the specimen) and plot the conventional $\sigma \sim \delta$ stress-strain diagram [1]. By using the “virtual extensometer” software option of the digital image correlation method, we recorded the relative elongation of the specimen as in the case of the strain-gauge extensometer. The results of measurements by the “virtual extensometer” were used to plot the $\sigma \sim \delta$ diagram (Fig. 3a), which practically coincides with the diagram constructed by the standard technique [6].

To plot the true fracture diagram [3], we continuously record the changes in the cross-sectional area of the specimen at the site of necking and determine the “running” relative narrowing ψ_i

$$\psi_i = \frac{F_0 - F_i}{F_0}, \psi_i = \frac{F_0 - F_i}{F_0} \tag{1}$$

where F_0 is the initial cross-sectional area of the specimen and F_i is its running value. We determined ψ_i by measuring the changes in the diameter of the specimen in the neck under loading and using the DIC method. By using the value of ψ_i , we find the true strain as follows:

$$e_i = \ln \frac{1}{1 - \psi_i} e_i = \ln \frac{1}{1 - \psi_i} \tag{2}$$

The true stresses S_i in the neck of the specimen are given by the formula:

$$S_i = \frac{P_i}{F_i} \tag{3}$$

Thus, we can construct the “true stress S –true strain e ” diagram [6].

At the same time, in testing the specimens, the true strain e was determined by the direct measurements of displacements at the site of necking. As shown earlier [6, 7], the local strain is equal to the true strain given by formula (2) under the conditions of its determination with the use of the optimal gauge length of displacements (for steel, it varies from 10 to 20 μm). According to the results of measurements, we plotted the true diagram, which practically coincides with the classical way of construction. The true diagrams were plotted for the solid reinforcement bar and specimens with diameters of 10 and 8 mm (Fig. 3b). The averaged mechanical characteristics determined in the tests are presented in Table 1.

Table 1. Mechanical Characteristics of the Material of Reinforcement

Type of the specimen	$\sigma_{0.2}$, MPa	σ_u , MPa	δ , %	S , MPa	e , %
I	570	650	14.4	920	95
II	482	550	15.0	770	119
III	395	450	16.2	600	146

The analysis of the results of our investigations shows that the ultimate strength σ_u for the reinforcement bar is higher by 15 and 30% than for the specimens of types II and III, respectively. At the same time, the relative elongation δ varies within the range 11%. The true fracture stresses S for the reinforcement bar are higher than for the specimens of types II and III by 15 and 34%, respectively. The value of S is higher than the conventional ultimate strength σ_u for all types of specimens by 30%. The true critical strain e is 7–9 times higher than the relative elongation δ and changes within the range 35% for different types of specimens.

Thus, the results of determination of the mechanical characteristics of specimens of different types made of the same reinforcement bar are noticeably different. The difference between their strain characteristics established according to the true stress–strain diagrams is especially pronounced. In general, as the strength characteristics σ_u and S increases, the strain characteristics δ and e decrease, i.e., the resistance of the material to brittle fracture becomes lower. The energy approach based on the use of the specific fracture energy, which is an invariant characteristic of strength of the material and characterizes its elastoplastic fracture most exactly [8, 9], gives the most objective information about the ability of the plastic material to resist fracture. As a result of the construction of true stress–strain diagrams, we can determine the specific strain energy for all types of specimens by the following formula:

$$W = \int_0^{\varepsilon} \sigma(\varepsilon) d\varepsilon W = \int_0^e S(e) de . \quad (4)$$

In the plots, the strain energy W corresponds to the area under the true S – e diagram. We assume that, after attainment of the critical value of strain energy, i.e., of the fracture energy, the material fails:

$$W(S, e) = W_C . \quad (5)$$

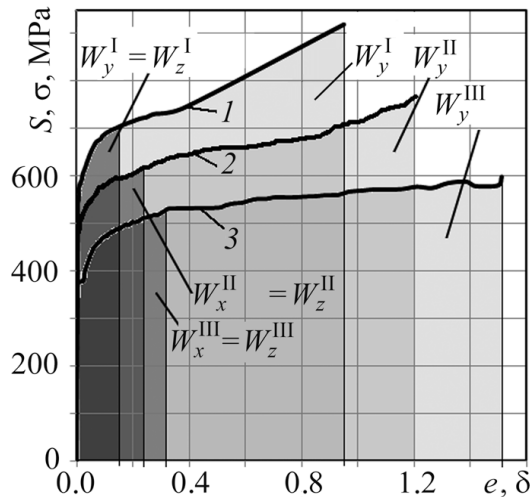


Fig. 4. Determination of the specific fracture energy from the true stress-strain diagrams of reinforcement: (1) untreated bar; (2) specimen with a diameter of 8 mm; (3) specimen with a diameter of 8 mm.

Table 2. True Strains, Stresses, and Specific Strain Energy of the Material of Reinforcement

Type of the specimen	e			S , MPa			W , MJ/m ³			
	e_{yc}	e_{xc}	e_{zc}	S_{yc}	S_{xc}	S_{zc}	W_{yc}	W_{xc}	W_{zc}	W_c
I	0.95	0.16	0.16	920	710	710	748.9	111.7	111.7	972.3
II	1.19	0.25	0.25	770	615	615	763.4	125.5	125.5	1014.4
III	1.46	0.32	0.32	600	530	530	781.9	150.6	150.6	1083.1

We also assume that the fracture energy of the material can be represented as the sum of components of the strain energy

$$W = W_x + W_y + W_z = W_c, \quad (6)$$

where W_y , W_x , and W_z are the strain energy in the directions of the coordinate Ox -, Oy -, and Oz -axes.

Thus, to determine the components of energy W_y , W_z , and W_x , it is necessary to plot the stress-strain diagrams in three main directions. We determine the strain e_y directly from the results of tensile testing of cylindrical specimens by the DIC method, whereas the strains e_x and e_z are found from the displacements along the Ox - and Oz - axes in the neck in the process of deformation of the specimen.

In view of the fact that, for cylindrical specimens, $e_x = e_z$, the strains e_x and e_z and the $S_y \sim e_y$ diagram can be used to find the true stresses S_x and S_z , under the assumption that the dependences of the strains on stresses are identical in all three directions because the material is isotropic.

The stress-strain diagrams for three types of specimens are shown in Fig. 4. The superscripts I–III for the components of energy W_x , W_y , and W_z correspond to the types of the specimens. The averaged values obtained as a result of testing of three specimens of each type are presented in Table 2.

It is easy to see that the fracture energy determined for different zones of the thermally hardened reinforcement bar varies by at most 10%. The analysis of the results of investigations shows that, in finding the load-bearing capacity of reinforced-concrete structural elements, it is necessary to take into account the variations both of the strength characteristics and of the strain characteristics depending on the type of the specimen. At the same time, the fracture energy determined according to the true diagrams is an invariant characteristic of the material, which should be used in calculations of this kind.

CONCLUSIONS

We show that the strength characteristics σ_u for specimens of different diameters made of thermally hardened reinforcement bars vary within 30%, whereas the strain characteristics vary within 11%. At the same time, the true stresses S vary within 34% and the true strains e vary within 35%. The specific fracture energy for all three types of specimens varies within 10%.

REFERENCES

1. GOST 1497-84. *Metals. Methods for Tensile Testing* [in Russian], Izd. Standartov, Moscow (1985).
2. G. S. Pisarenko and V. A. Strizhalo, *Experimental Methods in the Mechanics of Deformable Bodies* [in Russian], Naukova Dumka, Kiev (1986).
3. Ya. B. Fridman, *Mechanical Properties of Metals, Vol. 1: Deformation and Fracture* [in Russian], Mashinostroenie, Moscow (1974).
4. T. Chu, W. Ranson, and M. Sutton, "Applications of digital-image-correlation techniques to experimental mechanics," *Exp. Mech.*, **25**(3), 232–244 (1985).
5. B. Pan, K. M. Qian, H. M. Xie, and A. Asundi, "Two-dimensional digital image correlation for in-plane displacement and strain measurement: A review," *Meas. Sci. Technol.*, **20**(6), 062001–062007 (2009).
6. Yu. V. Mol'kov, "Application of the method of digital image correlation to the construction of stress–strain diagrams," *Fiz.-Khim. Mekh. Mater.*, **48**, No. 6, 121–125 (2012); **English translation: Mater. Sci.**, **48**, No. 6, 832–837 (2013).
7. Ya. L. Ivanyts'kyi, Yu. V. Mol'kov, P. S. Kun,' et al., "Determination of the local strains near stress concentrators by the digital image correlation technique," *Fiz.-Khim. Mekh. Mater.*, **50**, No. 4, 18–24 (2014); **English translation: Mater. Sci.**, **50**, No. 4, 488–495 (2014).
8. L. F. Gillemot, "Criterion of crack initiation and spreading," *Eng. Fract. Mech.*, **8**, 239–253 (1976).
9. H. J. Schindler, "Strain energy density as the link between global and local approach to fracture," in: K. Ravi-Chandar, et al., (editors), *Proc. of the 10th Internat. Conf. on Fracture*, Pergamon, Honolulu (2001), Reference ID: ICF 100494OR.